Insensitivity of the striped charge orders in IrTe₂ to alkali surface doping implies their structural origin

M. Rumo [1,*] A. Pulkkinen [1,2] B. Salzmann [1] G. Kremer [1] B. Hildebrand [1] K. Y. Ma,[3] F. O. von Rohr,[3]
C. W. Nicholson,[1] T. Jaouen,[4] and C. Monney[1,†]

[1]*Département de Physique and Fribourg Center for Nanomaterials, Université de Fribourg, CH-1700 Fribourg, Switzerland*
[2]*School of Engineering Science, LUT University, FI-53850, Lappeenranta, Finland*
[3]*Department of Chemistry, University of Zurich, CH-8057 Zurich, Switzerland*
[4]*Univ Rennes, CNRS, Institut de Physique de Rennes - UMR 6251, F-35000 Rennes, France*

We present a combined angle-resolved photoemission spectroscopy and low-energy electron diffraction (LEED) study of the prominent transition metal dichalcogenide IrTe₂ upon potassium (K) deposition on its surface. Pristine IrTe₂ undergoes a series of charge-ordered phase transitions below room temperature that are characterized by the formation of stripes of Ir dimers of different periodicities. Supported by density functional theory calculations, we first show that the K atoms dope the topmost IrTe₂ layer with electrons, therefore strongly decreasing the work function and shifting only the electronic surface states towards higher binding energy. We then follow the evolution of its electronic structure as a function of temperature across the charge-ordered phase transitions and observe that their critical temperatures are unchanged for K coverages of 0.13 and 0.21 monolayer. Using LEED we also confirm that the periodicity of the related stripe phases is unaffected by the K doping. We surmise that the charge-ordered phase transitions of IrTe₂ are robust against electron surface doping, because of its metallic nature at all temperatures, and due to the importance of structural effects in stabilizing charge order in IrTe₂.

I. INTRODUCTION

Low-dimensional transition metal dichalcogenides (TMDCs) are very attractive for study because high quality crystals of large size can be grown and exfoliated down to the monolayer (ML). They display a wide range of physical properties and complex phase diagrams including charge-density waves (CDWs) and superconductivity [1–6]. Many of these compounds have a relatively simple low-energy electronic structure with a few relevant bands and can be seen as model systems for small gap semiconductors [7], valleytronics [8–11], and also topological properties [12–14]. They have often been investigated by means of external perturbations, not only to understand their physical properties, but also to control them [15–18]. In this framework, *in situ* alkali deposition is an efficient and simple way to tune, suppress, or generate new ground states. It has been shown to have a strong impact on most CDW phases in TMDCs [19,20], to induce a surface semiconductor-semimetal transition in black phosphorus [21], or even to enhance the excitonic insulator phase in Ta₂NiSe₅ [22]. To date, there is no such study on IrTe₂, an enigmatic large spin-orbit coupling TMDC exhibiting a complex succession of charge-ordered phases as a function of temperature [23–26].

IrTe₂ undergoes several structural first-order phase transitions below room temperature (RT). The system goes from a trigonal unit cell of CdI₂ type ($P\bar{3}m1$) to a monoclinic unit cell ($P\bar{1}$) accompanied by a sudden jump in resistivity and magnetic susceptibility at $T_{c_1} = 278$ K [26,28–35]. In this first charge-ordered phase, one-dimensional stripes of Ir dimers [25,36] appear due to a large decrease of their bond length and lead to a $(5 \times 1 \times 5)$ superstructure [23,28,32,36–39]. Although the changes of the inplane bonding suggest a multicenter bond as a more complete description [40], for brevity, we will continue to use "dimers" throughout the text. A second phase transition occurs at $T_{c_2} = 180$ K, characterized by an $(8 \times 1 \times 8)$ superstructure. This has stimulated numerous scanning tunneling microscopy (STM) [24,28,37,41] and angle-resolved photoemission spectroscopy (ARPES) studies [18,26,28,42–44], which revealed additional periodicities and a surface periodicity (6×1) appearing after a third phase transition at $T_{c_3} = 165$ K. At low temperatures these phases coexist on the nanometer scale [25] therefore complicating the interpretation of ARPES data which averages over the beam area. Substantial changes to the material behavior are produced by doping: superconductivity is induced by partial substitution of Ir with Pt [3] or Pd [45], or by temperature quenching [16], while partial substitution of Te with Se induces charge order [23,38,41], further emphasizing the metastable nature of the material. Recently it has been shown that the application of uniaxial strain to IrTe₂ grants access to macroscopic regions of the (6×1) ground state and its corresponding topological states [18]. This stabilization was

---

*Corresponding author: maxime.rumo@unifr.ch
†Corresponding author: claude.monney@unifr.ch

found to be enabled by the strain-induced charge transfer from Ir to the out-of-plane antibonding Te orbitals, which modifies the energetic landscape of the competing phases. An open question is how the occurrence and periodicity of these different charge-ordered phases react to deposition of alkali atoms at the surface of $IrTe_2$, and whether a similar stabilizing effect as observed with strain may be achieved.

We report here on the effect of *in situ* potassium (K) deposited at RT on the electronic structure of $IrTe_2$ by means of ARPES. Combined with density functional theory (DFT) calculations, we establish that the K atoms give most of their electronic charge to the surface layer, resulting in a significant decrease of the work function. As the doping density increases, the surface electronic states are progressively lowered towards higher binding energies (BE). Although the K atoms modify the surface electronic structure, temperature-dependent ARPES shows that the critical temperatures of the phase transitions remain unaffected, while low-energy electron diffraction (LEED) measurements of the low-temperature charge-ordered phases confirm that the stripes periodicities remain unchanged. This demonstrates that alkali doping, which electronically populates states close to the Fermi level, is not sufficient to interfere with the bonding-antibonding molecular states relevant for the phase transition that occur far from the Fermi energy. Despite the fact that alkali doping affects only the surface, we observe that the surface reconstruction is similarly unchanged. This suggests that local lattice effects are central to understand the formation of charge-ordered phase transitions in $IrTe_2$.

II. METHODS

Single crystals of $IrTe_2$ were grown using the self-flux method [29,30]. They were characterized by magnetic susceptibility and resistivity measurements, which confirm that $T_{c_1} = 278$ K and $T_{c_2} = 180$ K [26]. Samples were cleaved at RT in vacuum at a pressure of about 10^{-8} mbar. During the photoemission measurements, the base pressure was better than 5×10^{-11} mbar. K deposition was achieved *in situ* by evaporation from a commercial SAES getter source in pressure below 5×10^{-10} mbar. The temperature-dependent ARPES study was carried out using a Scienta DA30 photoelectron analyzer and two different excitation sources, namely monochromatized He$_I$ radiation ($h\nu = 21.22$ eV) and a high-energy-resolution laser commercial setup (Harmonix, APE GmbH) generating 6.3 eV photons using harmonic generation from the output of an optical parametric oscillator pumped by a Paladin laser (Coherent, inc.) at 80 MHz. The total energy resolutions were about 5 and 3 meV at 21.2 and 6.3 eV photon energy, respectively, and the error on the sample temperature was estimated to be 5 K. Cooling of the sample was carried out at rates <3 K/min and each measurement was preceded by a pause of at least 10 min to ensure thermalization. Scanning tunneling microscopy (STM) measurements were performed on a commercial low-temperature STM (Scienta-Omicron) at 4.5 K in fixed current mode and with a bias voltage applied to the sample. The LEED patterns were recorded with a SPECS ErLEED at 64 eV.

DFT calculations with spin-orbit interaction were performed using the Vienna *ab initio* simulation package (VASP)

[46–49] within the projector augmented wave method [50] and the Perdew-Burke-Ernzerhof (PBE) functional [51]. The surface was modeled by a slab of three layers, with the bottom layer atoms fixed at bulk positions and the rest of the atom positions relaxed until the forces are <1 meV/Å. The K atoms were placed on the topmost surface, and dipole corrections were included to account for the adsorbate-induced dipole moment. The cutoff energy was set to 400 eV and the *k*-point grid spacing was <0.025 Å^{-1}. Band unfolding has been performed using the PYPROCAR code [52].

III. RESULTS

A. Potassium deposition characterization

We first address the influence of K deposition on the surface electronic structure of $IrTe_2$ at RT. Combining ARPES and STM measurements on the sample, we are able to estimate the K coverage as a function of exposure time to the K evaporation source. More details are available in Appendix A.

Figure 1(a) displays the evolution of the work function of $IrTe_2$ with K deposition. The work function ϕ, defined as the energy of the vacuum level E_{vac} with respect to the Fermi level E_F, is determined from the low-energy cutoff E_{cut} of the secondary photoelectron emission measured using 6.3 eV photons (see the inset), $\phi = h\nu - (E_F - E_{cut})$. With increasing K coverage, the work function decreases, and exhibits a saturation after a deposition of 0.2 monolayer (ML) (1 ML corresponds to one K atom per $IrTe_2$ surface unit cell). For coverages below 0.13 ML, a constant decrease of the work function is observed. In the inset are shown angle-integrated ARPES spectra of pristine $IrTe_2$ as well as $IrTe_2$ with the highest K doping used in this study. We have then performed DFT calculations to anticipate the influence of K deposition on the low energy surface electronic band structure of $IrTe_2$. Figure 1(b) displays the atomic structure of $IrTe_2$ with one K adatom on a (3×3) surface unit cell for a three-layer slab, corresponding to a 0.11 ML coverage. The structure has been relaxed and the optimal K adsorption site has been found to be on top of an Ir atom. The changes to the charge distribution induced by the K adatom are also shown on the same image. Our calculations demonstrate that only the surface charge distribution is modified by the K adsorption, and according to Bader analysis [53–56], each K adatom gives about $0.63e^-$ to the first $IrTe_2$ surface layer, corresponding to $0.07e^-$ per (1×1) unit cell on average.

The effect of the strong electron doping induced by adsorption of 0.11 ML of K at the surface is also visible on the calculated electronic band structure in Fig. 1(c) along the A-L direction of the three-dimensional (3D) Brillouin zone (BZ) [see Fig. 2(a)]. The red and black band structures correspond to the pristine and K-doped $IrTe_2$ structures, respectively. The main changes occur within the first eV below the Fermi level E_F with a shift of the surface-related electronic states towards higher BE. In particular, the band located at the A point around 0.8 eV below E_F is shifted by almost 100 meV down to high BE and is flattened. This band is known to be a surface state (SS) [14,26] and is consequently strongly affected by the surface doping, as discussed below.
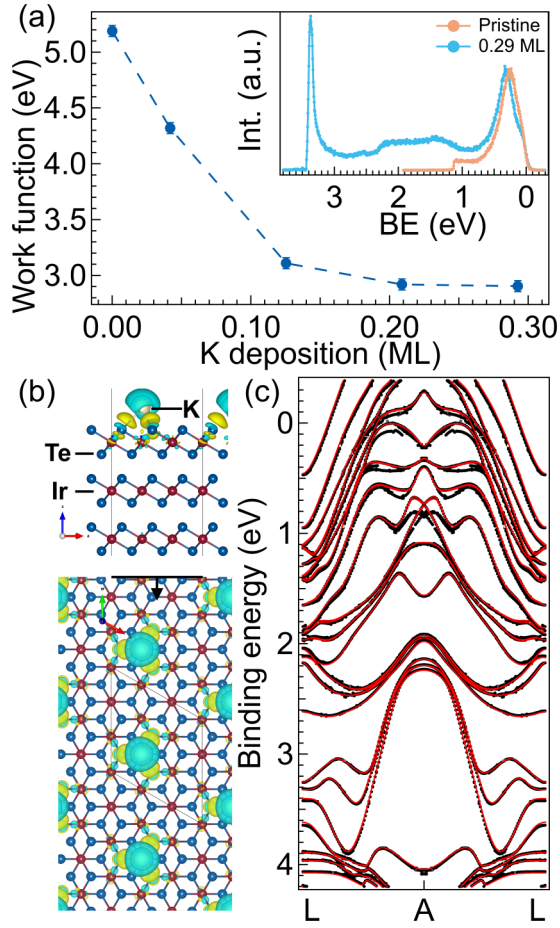
FIG. 1. (a) Evolution of the work function of IrTe$_2$ as a function of K coverage. The inset shows energy distribution curves (EDCs) measured at RT with a photon energy of $h\nu = 6.3$ eV on a pristine crystal and 0.29 ML K-doped crystal along the AL direction. (b) Side and top views of the IrTe$_2$ atomic structure with a (3×3) K adlayer on the surface. The light blue isosurface refers to the missing charge and the yellow isosurface to the gained charge at $0.001 e^-/a_0^3$ [27], where a_0 is the Bohr radius. (c) Band structure calculation of the pristine IrTe$_2$ (red) and with a K adlayer as shown in (b) (black).

B. Electronic structure at room temperature

We have performed ARPES measurements as a function of K deposition at RT to further discriminate the changes in the electronic structure of IrTe$_2$. Figure 2(a) presents the 3D BZ and its surface projection. A RT Fermi surface (integrated over 0.05 eV around E_F) is shown in Fig. 2(b), obtained with a photon energy $h\nu = 21.22$ eV. At this photon energy, states close to the ALH plane are probed [43,44,57]. In Fig. 2(c) ARPES spectra taken at RT along the AL direction for a pristine crystal, as well as for 0.04, 0.13, 0.21, and 0.29 ML K-doped crystals, are displayed. Corresponding energy distribution curves (EDC) integrated on a small momentum range (± 0.09 Å^{-1}) around A are shown in Fig. 2(d). On the pristine crystal [Fig. 2(c), left panels], the electronic bands are sharp and, by comparison with the literature [14,26,42], we can identify the presence of bulk state B1 just below E_F, a second bulk band B2, and an intense surface state SS at about 1 eV BE [26]. With the increase of K doping, the surface

state SS flattens and shifts towards higher BE from 1 (pristine crystal) to 1.2 eV (0.29 ML K-doped crystal) [also see the corresponding EDCs integrated around A in Fig. 2(d)]. Note that a second surface state SS2 near E_F exhibits a similar shift to higher BE [see Fig. 2(c)]. These observations are in line with the prediction obtained from our DFT calculations of Fig. 1(c), especially with respect to the surface states SS and SS2. Figure 2(e) reports the relative shift of the surface state SS (ΔE_{SS}) at A as a function of K doping [see also the blue markers in Fig. 2(c)], which follows the same trend as the work function [see Fig. 1(a)].

Overall, the K adsorption at the surface of metallic IrTe$_2$ produces a shift of the surface states, as already observed in numerous materials [58–60]. However, IrTe$_2$ is a singular material since it undergoes a series of charge-ordered phase transitions upon cooling [24,26,28,37,42]. Consequently, a crucial point to address is the impact of K surface doping on such structural instabilities.

C. Temperature dependence in ARPES

We have thus performed temperature-dependent ARPES measurements with a particular focus on the energy position of the surface state at around 1 eV BE that can be used as a marker of the phase transitions [26], since its BE depends strongly on the Ir-Ir dimer length in the stripe phases. In Fig. 3(a) we recall schematically the structure of the basic building blocks for the Ir atoms in the different phases in IrTe$_2$. The (1×1) phase is composed only of equivalent atoms, leading to the surface state SS at about 1 eV BE. In the (5×1) phase, five atoms split into two dimerized Ir atoms (one dimer) and three undimerized atoms [Fig. 3(a)]. This leads to a splitting of the surface state SS into a contribution due to the dimerized Ir atoms, named SSD, at higher binding energy, and a contribution due to the three undimerized Ir atoms, named SS3. In the (8×1) and in the (6×1) phases [Fig. 3(a)], the sequence of Ir atoms changes further, implying a different combination of dimerized and undimerized atoms. At the same time, the Ir-Ir dimer length has been shown to reduce further across these phase transitions [23,25].

Figure 3(b) displays ARPES spectra taken at 295 K $> T_{c_1}$, $T_{c_1} > 200$ K $> T_{c_2}$, and 30 K $< T_{c_2}$, along AL direction for a K coverage of 0.13 ML (see all ARPES data in Appendix B). At 295 K, sharp electronic states are clearly observed on the left panel. The surface state SS is easily distinguishable at a BE of 1.14 eV. For temperatures below T_{c1}, the electronic states become more intricate due to the appearance of new translational symmetry of the charge-ordered phases of mixed orientations [25]. A multitude of folded bands can be identified, especially in the BE range between E_F and 2.0 eV, see Fig. 3(b). At 200 K, in the (5×1) phase, the surface state SS is split into two states, namely SS3 and SSD, the BE of the latter being now 1.4 eV. At 30 K, in the (6×1)-dominated phase [see right panels in Fig. 3(b)], SSD shifts further to higher BE reaching 1.49 eV. Figure 3(c) shows EDCs at the energy of the surface state integrated on a small momentum range (± 0.09 Å^{-1}) around A together with the corresponding fits, consisting of a single Gauss function, for temperatures down to 30 K. The resulting shift of the surface state SSD in BE, ΔE_{SSD}, is defined as the difference between the surface state
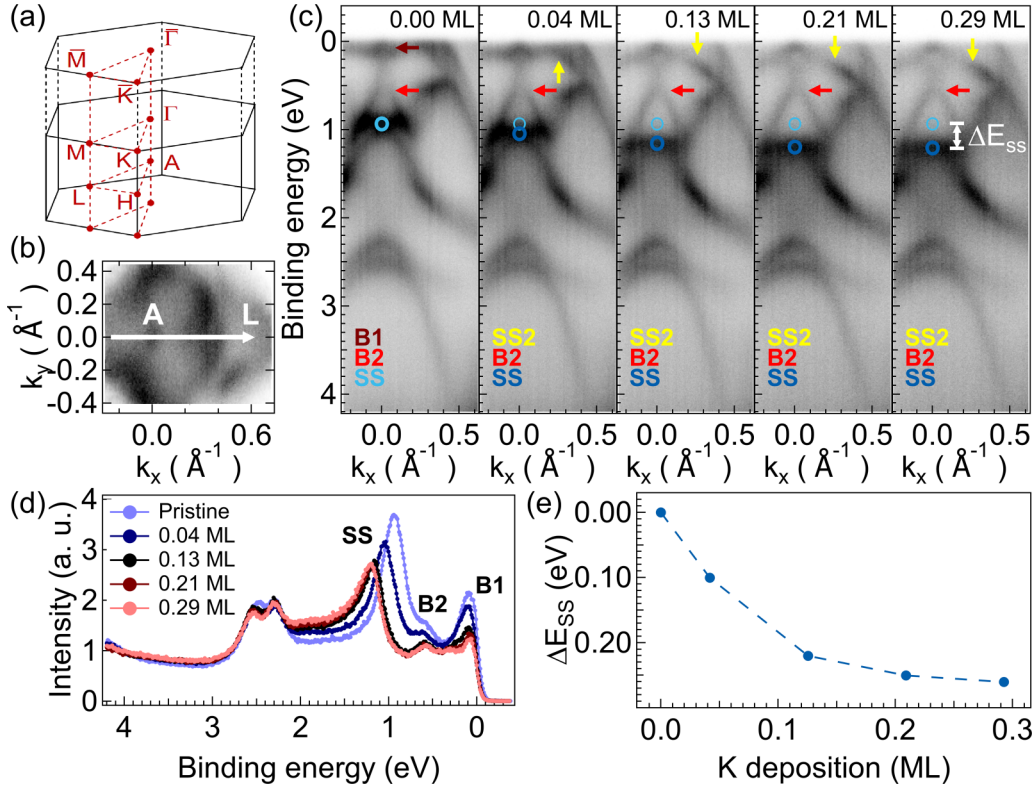
FIG. 2. (a) The Brillouin zone of IrTe$_2$. (b) Fermi surface of IrTe$_2$ for $h\nu = 21.22$ eV taken at 295 K. (c) ARPES spectra measured along AL direction for $h\nu = 21.22$ eV for a pristine, 0.04, 0.13, 0.21, and 0.29 ML K-doped crystals. (d) EDCs for the pristine and K-doped crystals (integrated ± 0.09 Å^{-1} around A along AL direction). (e) Binding energy shift of the surface state SS measured in ARPES as a function of K doping.

SS RT value for a given doping and the surface state SSD value at a temperature T for the same doping [see also the colored markers in Fig. 3(b)]. It is displayed for the pristine crystal (same data as in Ref. [26]) as well as for the present 0.13 ML K-doped crystal and for an additional doping of 0.21 ML as a function of temperature in Fig. 3(d). It allows us to compare directly the evolution of SSD with and without potassium.

Interestingly, the magnitudes of ΔE_{SSD} upon cooling through all three first-order phase transitions (278, 180, and 165 K) for the 0.13 ML K-doped crystal are not only nearly indistinguishable from pristine IrTe$_2$, but also from a more K-doped sample (0.21 ML). This indicates that the phase transitions are remarkably insensitive to K deposition at these values of K doping.
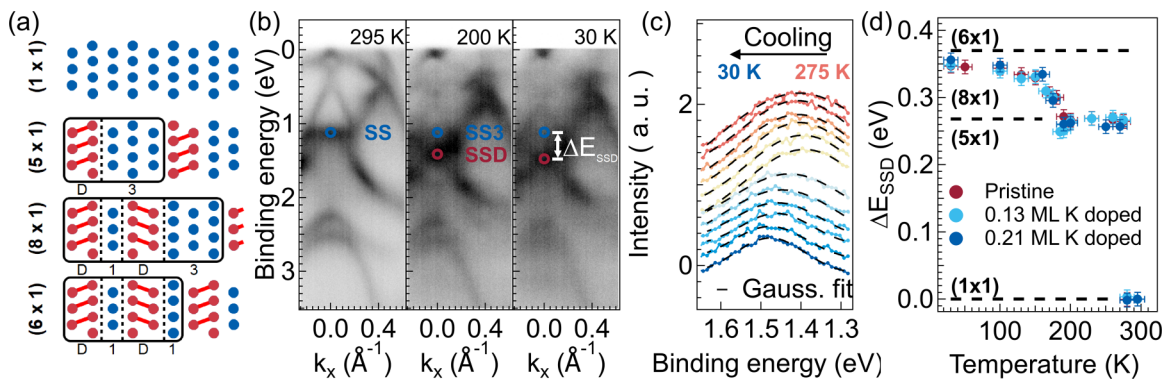

FIG. 3. (a) Structural models of the Ir atomic planes for the different charge-ordered phases. (b) ARPES spectra measured along AL direction for $h\nu = 21.22$ eV at three different temperatures for 0.13 ML K-doped crystal of IrTe$_2$. (c) Temperature-dependent EDCs upon cooling (integrated ± 0.09 Å^{-1} around A along AL direction). (d) RT relative binding energy shift of the surface state SSD measured in ARPES as a function of temperature for a pristine crystal, 0.13 and 0.21 ML K-doped crystals.
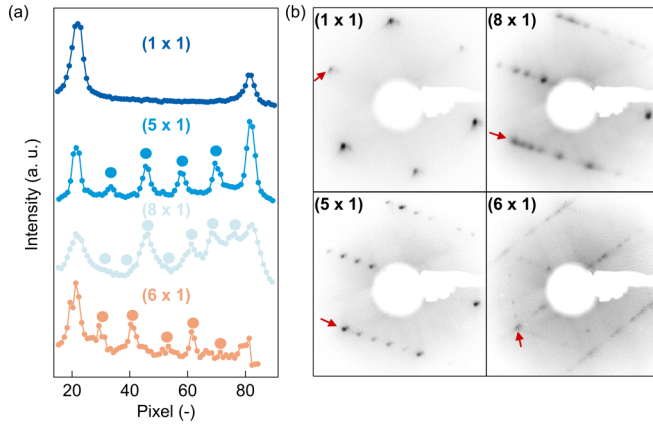
FIG. 4. (a) Line profiles of LEED images shown in (b). (b) Raw LEED images of a 0.13 ML K-doped IrTe$_2$ crystal in the (1×1) phase at 295 K, (5×1) phase at 230 K, (8×1) phase at 170 K, and (6×1) phase at 30 K. All images were obtained using 64 eV electron energy.

D. Temperature dependence in LEED

To support the conclusions drawn from ARPES, we have also checked the periodicities of the stripe phases of the 0.13 ML K-doped crystal of IrTe$_2$ with LEED. Figure 4(a) displays the line profiles of LEED images taken at different temperatures (upon cooling) specific to the different phases of IrTe$_2$, see Fig. 4(b). They confirm the presence of the (1×1) phase at 295 K, the (5×1) phase at 230 K, the (8×1) phase at 170 K, and the (6×1) phase at 30 K. Note that due to the unavoidable mixture of domains of different orientations [61,62], lines of superstructure spots are observed in the threefold symmetry equivalent directions [see in particular the LEED image at 30 K for the (6×1) phase]. Furthermore, below T_{c_3}, we observe coexistence of domains of the (8×1) phase and of the (6×1) phase (see Appendix B), a pattern already observed for pristine crystals [26,61]. Our complementary LEED study therefore confirms that the deposition of K atoms does not change the periodicities of the stripe phases observed across the phase transitions at the surface of IrTe$_2$.

IV. DISCUSSION

In this work we report that K doping shifts the surface states SS at RT to higher BE, without inducing surface reconstruction (see LEED image at RT Fig. 4). This energy shift is due to a decrease of the surface potential, as observed for instance on the Au(111) surface [63], and is therefore not related to any dimerization. This is further confirmed by the absence of the split surface state SSD at RT (see Fig. 2). However, the energy shift of the surface state of the dimerized atoms, SSD, at low temperature across the phase transitions (see Fig. 3) does not vary with the K coverage used in this work. As motivated in our previous work [26], this means that the dimer length does not change and that the charge-ordered phase transitions are not modified by the surface K doping.

In contrast, many layered materials turn out to be very sensitive to alkali doping. For instance, the CDW phase in the TMDC TiSe$_2$ is already completely suppressed at about 0.1 ML of Rb coverage [19]. The band gap of the semiconducting layered-material black phosphorous is very sensitive to alkali doping, already decreasing above 0.1 ML and this material has been shown to undergo a semiconductor-semimetal transition at 0.35 ML [21]. The same effect has been discovered also in Ta$_2$NiSe$_5$ [22], for which a semiconductor-semimetal transition occurs at about 0.15 ML of K doping [64]. These recent results on low-dimensional layered materials emphasize the surprising insensitivity of IrTe$_2$ to K doping at low coverages.

What is then the reason for this robustness of the surface transitions in IrTe$_2$? IrTe$_2$ has a metallic behavior above and below the phase transitions, with a significant density of states maintained at the Fermi level [29,36], in contrast with the materials mentioned above. This is due to the fact that a dramatic reduction of density of states is observed only for the bonding and antibonding dimer states that are not lying close to E_F [36,40,65,66]. Away from these dimer states the density of states is insignificantly affected by the phase transitions [36]. This naturally makes the charge-ordered phase transitions in IrTe$_2$ insensitive to carrier doping, for three reasons. (1) Screening of the electric field of the ionized doping atoms is more efficient for a metallic surface. This excludes the possibility of a large unscreened electric field near the surface, which is central to the phase transition in black phosphorus for instance [21]. (2) When electron doping changes the low-energy band structure, and thus the corresponding Fermi surface shape, it can significantly alter the electronic susceptibility of materials, reducing their tendency to instabilities, as for instance in TiSe$_2$ [20] or Ta$_2$NiSe$_5$ [22]. This mechanism is often the cause of the suppression of a collective instability, like a charge-density wave, by alkali doping. However, the low-energy electronic structure of IrTe$_2$ is little modified by a given electron doping density in a rigid band model picture, since the high density of states at E_F can easily accommodate the doping electrons. (3) Finally, the doping charge does not populate the antibonding states that are further away from E_F, since the nonbonding states near E_F likely capture the K doping electron. This prevents the destabilization of Ir dimers. Furthermore, we recall here that our DFT calculations indicate that the charge transfer from the K adatom affects only the top surface layer and mainly dopes the surface states, a fact confirmed by our ARPES data, so that the bulk electronic structure stays unchanged. We further emphasize that, despite this surface doping, it is surprising that the (6×1) phase transition, which occurs only at the surface, is not affected. It demonstrates that purely electronic doping is not the most efficient way to destabilize the charge-ordered phases of IrTe$_2$. Therefore, our results support the idea that the instability is driven by a local mechanism mainly involving the atoms forming the dimers, stabilized by a large electronic energy gain due to the creation of the bonding-antibonding states of these dimers [23,36,40].

In contrast, recent literature reveals that structural perturbation, as induced by chemical substitution [3,6,38] or applied strain [18], is much more efficient at altering the phase diagram. More specifically for 4% of Pt or Pd substitution, which kills the charge order in favor of superconductivity, a gain of $0.04 e^-$ per unit cell throughout the crystal is achieved, while in our case $0.07 e^-$ per unit cell localized at the surface is observed from our calculations. However, the chemical substitution causes a local strain in the lattice. For

example, Pd has an atomic size difference of 1% with Te, which creates distortions in the lattice, which itself contributes to the phase transitions. This is much greater than the 0.1% mechanical strain which is observed to stabilize the (6×1) phase. The phase transitions are strongly disturbed in these particular cases while pure electronic doping is unable to induce such an effect. This is consistent with the results of a recent time-resolved ARPES study [67] that concluded that infrared photoexcitation cannot efficiently trigger the phase transition and that only a partial photoinduced phase transition occurs, driven by the transient heating of the lattice.

V. CONCLUSION

In this work we have studied the influence of K doping on IrTe$_2$ with ARPES and LEED, supported by DFT calculations. We have performed a detailed and systematic analysis as a function of K deposition at RT and we have probed the occurrence of charge-ordered phases as a function of temperature. We have shown that the perturbation by electronic doping from the alkali atoms has no effect on the charge-ordered phase transitions at the surface of IrTe$_2$. This emphasizes the important role of the structural component in the stabilization of these phases. In this framework, it will be particularly interesting to test the stability of the charge-ordered phases of IrTe$_2$ in the limit of a single monolayer or within van der Waals heterostructures.

ACKNOWLEDGMENTS

FIG. 6. (a) Lines profiles of LEED images shown in (b). (b) LEED image from a 0.13 ML K-doped crystal of IrTe$_2$ in the (8×1) and (6×1) phases at 30 K. All images were obtained using 64 eV electron energy.

APPENDIX A: K DEPOSITION CALIBRATION

Figure 5 shows a high-resolution STM image taken on a K-doped IrTe$_2$ crystal of the occupied states at a bias voltage of $V_{bias} = -200$ mV and a constant current mode of $I = 0.2$ nA with atomic resolution. The K deposition was performed at RT. The STM image (Fig. 5) reveals the presence of adsorbed K atoms at the surface as bright protrusions on top of the low temperature reconstruction of IrTe$_2$. From the statistics made on a few images, a K coverage of 0.01 ML is estimated for an exposition time to the SAES getter source of 30 s (one K atom per IrTe$_2$ surface unit cell at RT is defined as 1 ML of K atom).

We caution that this STM measurement reveals only adsorbed K atoms at the surface of IrTe$_2$. However, intercalation of K atoms in the van der Waals gap could also occur in parallel to adsorption, as reported in the literature for TaS$_2$ or graphite [19,68,69]. We stress that the distance between two sandwiches of IrTe$_2$ (interlayer spacing) is smaller (about 2.7 Å) than for most TMDCs and for graphite (3.3 Å). Therefore we expect alkali intercalation to be unfavorable for the present case.
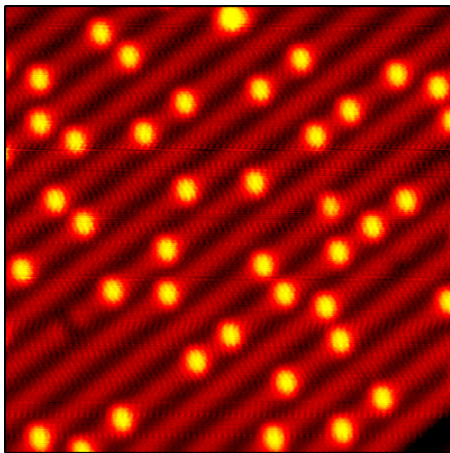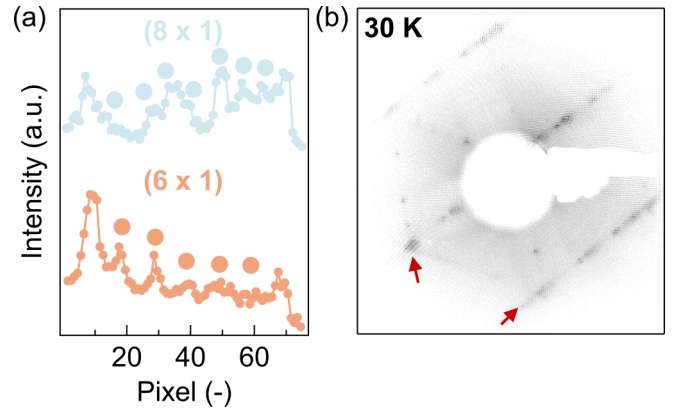

FIG. 5. 19.7×19.7 nm^2 constant current mode STM image of a 0.01 ML K-doped IrTe$_2$ sample, $V_{bias} = -200$ mV, $I = 0.2$ nA.

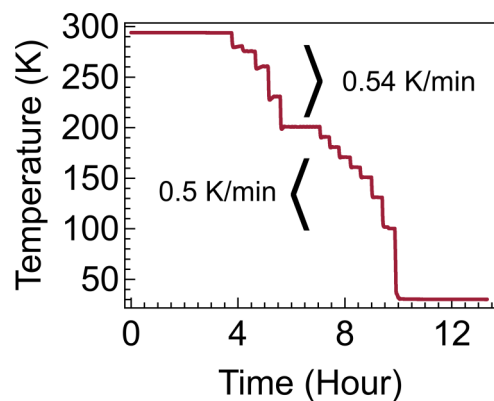
FIG. 7. Temperature of the sample as a function of time during the temperature dependence study.
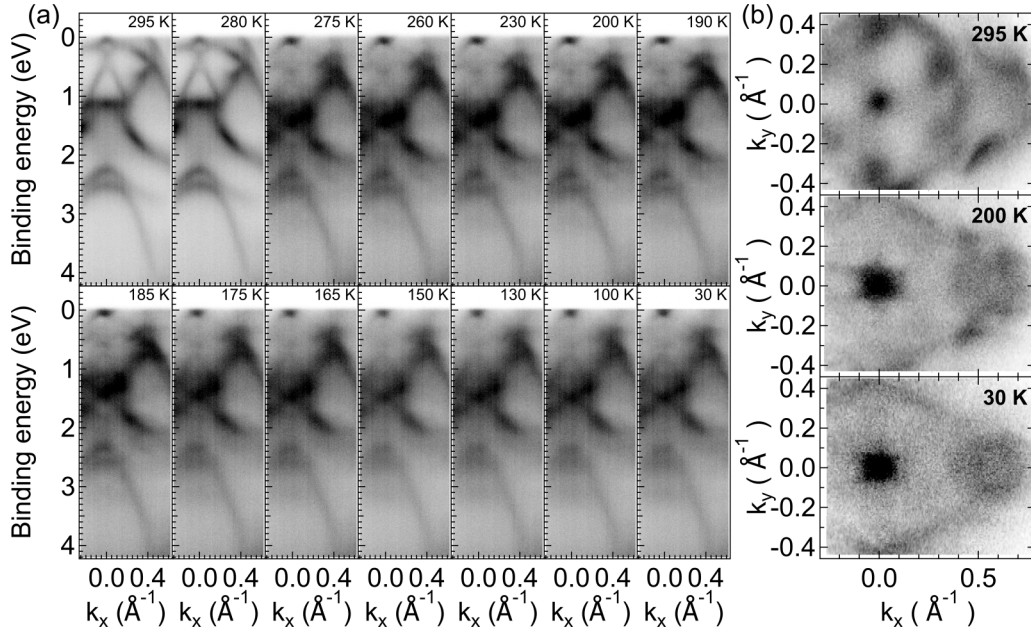
FIG. 8. (a) ARPES spectra of a 0.13 ML K-doped IrTe$_2$ crystal measured along AL direction with a photon energy of $h\nu = 21.22$ eV upon cooling. (b) Fermi surfaces of a 0.13 ML K-doped IrTe$_2$ crystal integrated over 0.05 eV around E_F at different temperatures upon cooling.

APPENDIX B: SUPPLEMENTARY DATA FOR THE TEMPERATURE DEPENDENT STUDY

Figure 6 displays a LEED image of the 0.13 ML K-doped IrTe$_2$ showing both the (8×1) and the (6×1) phases at 30 K, as observed in the pristine IrTe$_2$ case for the same temperature.

Figure 7 displays the evolution of the temperature of the sample during the temperature dependent ARPES measurements. The cooling rate is less than 3 K/min and on average less than 0.55 K/min.

Figure 8(a) shows ARPES spectra taken at different temperatures during the cooling process, 295, 280, 275, 260, 230, 200, 190, 185, 175, 165, 150, 130, 100, and 30 K on a 0.13 ML K-doped crystal of IrTe$_2$. The evolution of the electronic structure of a 0.13 ML K-doped crystal of IrTe$_2$ can be observed and in particular the shift of the surface state as a function of temperature. Figure 8(b) displays Fermi surfaces of a 0.13 ML K-doped IrTe$_2$ crystal at different temperatures.

[1] K. Rossnagel, J. Phys.: Condens. Matter **23**, 213001 (2011).

[2] M. D. Johannes and I. I. Mazin, Phys. Rev. B **77**, 165135 (2008).

[3] S. Pyon, K. Kudo, and M. Nohara, J. Phys. Soc. Jpn. **81**, 053701 (2012).

[4] E. Morosan, H. W. Zandbergen, B. S. Dennis, J. W. G. Bos, Y. Onose, T. Klimczuk, A. P. Ramirez, N. P. Ong, and R. J. Cava, Nat. Phys. **2**, 544 (2006).

[5] B. Sipos, A. F. Kusmartseva, A. Akrap, H. Berger, L. Forró, and E. Tutiš, Nat. Mater. **7**, 960 (2008).

[6] H. Yang, S. W. Kim, M. Chhowalla, and Y. H. Lee, Nat. Phys. **13**, 931 (2017).

[7] A. Chernikov, T. C. Berkelbach, H. M. Hill, A. Rigosi, Y. Li, O. B. Aslan, D. R. Reichman, M. S. Hybertsen, and T. F. Heinz, Phys. Rev. Lett. **113**, 076802 (2014).

[8] K. F. Mak, K. He, J. Shan, and T. F. Heinz, Nat. Nanotechnol. **7**, 494 (2012).

[9] H. Zeng, J. Dai, W. Yao, D. Xiao, and X. Cui, Nat. Nanotechnol. **7**, 490 (2012).

[10] J. M. Riley, F. Mazzola, M. Dendzik, M. Michiardi, T. Takayama, L. Bawden, C. Granerød, M. Leandersson, T. Balasubramanian, M. Hoesch et al., Nat. Phys. **10**, 835 (2014).

[11] R. Bertoni, C. W. Nicholson, L. Waldecker, H. Hübener, C. Monney, U. De Giovannini, M. Puppin, M. Hoesch, E. Springate, R. T. Chapman et al., Phys. Rev. Lett. **117**, 277201 (2016).

[12] A. Tamai, Q. S. Wu, I. Cucchi, F. Y. Bruno, S. Riccò, T. K. Kim, M. Hoesch, C. Barreteau, E. Giannini, C. Besnard et al., Phys. Rev. X **6**, 031021 (2016).

[13] Y. Wu, D. Mou, N. H. Jo, K. Sun, L. Huang, S. L. Bud'ko, P. C. Canfield, and A. Kaminski, Phys. Rev. B **94**, 121113(R) (2016).

[14] M. S. Bahramy, O. J. Clark, B.-J. Yang, J. Feng, L. Bawden, J. M. Riley, I. Markovic, F. Mazzola, V. Sunko, D. Biswas et al., Nat. Mater. **17**, 21 (2017).

[15] L. Stojchevska, I. Vaskivskyi, T. Mertelj, P. Kusar, D. Svetin, S. Brazovskii, and D. Mihailovic, Science **344**, 177 (2014).

[16] H. Oike, M. Kamitani, Y. Tokura, and F. Kagawa, Sci. Adv. **4**, eaau3489 (2018).

[17] E. J. Sie, C. M. Nyby, C. D. Pemmaraju, S. J. Park, X. Shen, J. Yang, M. C. Hoffmann, B. K. Ofori-Okai, R. Li, A. H. Reid et al., Nature (London) **565**, 61 (2019).

[18] C. W. Nicholson, M. Rumo, A. Pulkkinen, G. Kremer, B. Salzmann, M.-L. Mottas, B. Hildebrand, T. Jaouen, T. K. Kim, S. Mukherjee et al., Commun. Mater. **2**, 25 (2021).

[19] K. Rossnagel, New J. Phys. **12**, 125018 (2010).

[20] T. Jaouen, M. Rumo, B. Hildebrand, M. L. Mottas, C. W. Nicholson, G. Kremer, B. Salzmann, F. Vanini, C. Barreteau, E. Giannini *et al.*, arXiv:1911.06053.

[21] J. Kim, S. S. Baik, S. H. Ryu, Y. Sohn, S. Park, B.-G. Park, J. Denlinger, Y. Yi, H. J. Choi, and K. S. Kim, Science **349**, 723 (2015).

[22] K. Fukutani, R. Stania, J. Jung, E. F. Schwier, K. Shimada, C. I. Kwon, J. S. Kim, and H. W. Yeom, Phys. Rev. Lett. **123**, 206401 (2019).

[23] G. L. Pascut, T. Birol, M. J. Gutmann, J. J. Yang, S.-W. Cheong, K. Haule, and V. Kiryukhin, Phys. Rev. B **90**, 195122 (2014).

[24] T. Mauerer, M. Vogt, P.-J. Hsu, G. L. Pascut, K. Haule, V. Kiryukhin, J. Yang, S.-W. Cheong, W. Wu, and M. Bode, Phys. Rev. B **94**, 014106 (2016).

[25] P.-J. Hsu, T. Mauerer, M. Vogt, J. J. Yang, Y. S. Oh, S.-W. Cheong, M. Bode, and W. Wu, Phys. Rev. Lett. **111**, 266401 (2013).

[26] M. Rumo, C. W. Nicholson, A. Pulkkinen, B. Hildebrand, G. Kremer, B. Salzmann, M.-L. Mottas, K. Y. Ma, E. L. Wong, M. K. L. Man *et al.*, Phys. Rev. B **101**, 235120 (2020).

[27] K. Momma and F. Izumi, J. Appl. Crystallogr. **44**, 1272 (2011).

[28] K.-T. Ko, H.-H. Lee, D.-H. Kim, J.-J. Yang, S.-W. Cheong, M. J. Eom, J. S. Kim, R. Gammag, K.-S. Kim, H.-S. Kim *et al.*, Nat. Commun. **6**, 7342 (2015).

[29] A. F. Fang, G. Xu, T. Dong, P. Zheng, and N. L. Wang, Sci. Rep. **3**, 1153 (2013).

[30] S. Jobic, P. Deniard, R. Brec, J. Rouxel, A. Jouanneaux, and A. N. Fitch, Z. Anorg. Allg. Chem. **598**, 199 (1991).

[31] N. Matsumoto, K. Taniguchi, R. Endoh, H. Takano, and S. Nagata, J. Low Temp. Phys. **117**, 1129 (1999).

[32] T. Toriyama, M. Kobori, T. Konishi, Y. Ohta, K. Sugimoto, J. Kim, A. Fujiwara, S. Pyon, K. Kudo, and M. Nohara, J. Phys. Soc. Jpn. **83**, 033701 (2014).

[33] S. Koley, Solid State Commun. **247**, 40 (2016).

[34] B. Li, G. Huang, J. Sun, and Z. Xing, Sci. Rep. **4**, 6433 (2014).

[35] E. Paris, B. Joseph, A. Iadecola, C. Marini, H. Ishii, K. Kudo, S. Pascarelli, M. Nohara, T. Mizokawa, and N. L. Saini, Phys. Rev. B **93**, 134109 (2016).

[36] G. L. Pascut, K. Haule, M. J. Gutmann, S. A. Barnett, A. Bombardi, S. Artyukhin, T. Birol, D. Vanderbilt, J. J. Yang, S.-W. Cheong *et al.*, Phys. Rev. Lett. **112**, 086402 (2014).

[37] Q. Li, W. Lin, J. Yan, X. Chen, A. G. Gianfrancesco, D. J. Singh, D. Mandrus, S. V. Kalinin, and M. Pan, Nat. Commun. **5**, 5358 (2014).

[38] Y. S. Oh, J. J. Yang, Y. Horibe, and S.-W. Cheong, Phys. Rev. Lett. **110**, 127209 (2013).

[39] K. Takubo, R. Comin, D. Ootsuki, T. Mizokawa, H. Wadati, Y. Takahashi, G. Shibata, A. Fujimori, R. Sutarto, F. He *et al.*, Phys. Rev. B **90**, 081104(R) (2014).

[40] G. Saleh and S. Artyukhin, J. Phys. Chem. Lett. **11**, 2127 (2020), pMID: 32079398.

[41] J. Dai, K. Haule, J. J. Yang, Y. S. Oh, S.-W. Cheong, and W. Wu, Phys. Rev. B **90**, 235121 (2014).

[42] H. Lee, K.-T. Ko, K. Kim, B.-G. Park, J. Yang, S.-W. Cheong, and J.-H. Park, Europhys. Lett. **120**, 47003 (2017).

[43] D. Ootsuki, S. Pyon, K. Kudo, M. Nohara, M. Horio, T. Yoshida, A. Fujimori, M. Arita, H. Anzai, H.

[44] Namatame *et al.*, J. Phys. Soc. Jpn. **82**, 093704 (2013).

[44] D. Ootsuki, H. Ishii, K. Kudo, M. Nohara, M. Arita, H. Namatame, M. Taniguchi, N. L. Saini, and T. Mizokawa, J. Phys. Chem. Solids **128**, 270 (2019).

[45] J. J. Yang, Y. J. Choi, Y. S. Oh, A. Hogan, Y. Horibe, K. Kim, B. I. Min, and S.-W. Cheong, Phys. Rev. Lett. **108**, 116402 (2012).

[46] G. Kresse and J. Hafner, Phys. Rev. B **47**, 558 (1993).

[47] G. Kresse and J. Hafner, Phys. Rev. B **49**, 14251 (1994).

[48] G. Kresse and J. Furthmüller, Comput. Mater. Sci. **6**, 15 (1996).

[49] G. Kresse and J. Furthmüller, Phys. Rev. B **54**, 11169 (1996).

[50] G. Kresse and D. Joubert, Phys. Rev. B **59**, 1758 (1999).

[51] J. P. Perdew, K. Burke, and M. Ernzerhof, Phys. Rev. Lett. **77**, 3865 (1996).

[52] U. Herath, P. Tavadze, X. He, E. Bousquet, S. Singh, F. Muñoz, and A. H. Romero, Comput. Phys. Commun. **251**, 107080 (2020).

[53] W. Tang, E. Sanville, and G. Henkelman, J. Phys.: Condens. Matter **21**, 084204 (2009).

[54] E. Sanville, S. D. Kenny, R. Smith, and G. Henkelman, J. Comput. Chem. **28**, 899 (2007).

[55] G. Henkelman, A. Arnaldsson, and H. Jónsson, Computat. Mater. Sci. **36**, 354 (2006).

[56] M. Yu and D. R. Trinkle, J. Chem. Phys. **134**, 064111 (2011).

[57] D. Ootsuki, T. Toriyama, M. Kobayashi, S. Pyon, K. Kudo, M. Nohara, T. Sugimoto, T. Yoshida, M. Horio, A. Fujimori *et al.*, J. Phys. Soc. Jpn. **83**, 033704 (2014).

[58] M. A. Hossain, J. D. F. Mottershead, D. Fournier, A. Bostwick, J. L. McChesney, E. Rotenberg, R. Liang, W. N. Hardy, G. A. Sawatzky, I. S. Elfimov *et al.*, Nat. Phys. **4**, 527 (2008).

[59] T. J. Boyle, A. Rossi, M. Walker, P. Carlson, M. K. Miller, J. Zhao, P. Klavins, C. Jozwiak, A. Bostwick, E. Rotenberg *et al.*, Phys. Rev. B **100**, 081105(R) (2019).

[60] G. Kremer, T. Jaouen, B. Salzmann, L. Nicolaï, M. Rumo, C. W. Nicholson, B. Hildebrand, J. H. Dil, J. Minár, G. Springholz *et al.*, Phys. Rev. Research **2**, 033115 (2020).

[61] C. Chen, J. Kim, Y. Yang, G. Cao, R. Jin, and E. W. Plummer, Phys. Rev. B **95**, 094118 (2017).

[62] T. Machida, Y. Fujisawa, K. Igarashi, A. Kaneko, S. Ooi, T. Mochiku, M. Tachiki, K. Komori, K. Hirata, and H. Sakata, Phys. Rev. B **88**, 245125 (2013).

[63] F. Forster, A. Bendounan, J. Ziroff, and F. Reinert, Surf. Sci. **600**, 3870 (2006).

[64] L. Chen, T. T. Han, C. Cai, Z. G. Wang, Y. D. Wang, Z. M. Xin, and Y. Zhang, Phys. Rev. B **102**, 161116(R) (2020).

[65] S.-i. Ideta, D. Zhang, A. G. Dijkstra, S. Artyukhin, S. Keskin, R. Cingolani, T. Shimojima, K. Ishizaka, H. Ishii, K. Kudo *et al.*, Sci. Adv. **4**, eaar3867 (2018).

[66] K. Kim, S. Kim, K.-T. Ko, H. Lee, J.-H. Park, J. J. Yang, S.-W. Cheong, and B. I. Min, Phys. Rev. Lett. **114**, 136401 (2015).

[67] C. Monney, A. Schuler, T. Jaouen, M.-L. Mottas, T. Wolf, M. Merz, M. Muntwiler, L. Castiglioni, P. Aebi, F. Weber *et al.*, Phys. Rev. B **97**, 075110 (2018).

[68] M. Caragiu and S. Finberg, J. Phys.: Condens. Matter **17**, R995 (2005).

[69] C. Ramírez, R. Adelung, L. Kipp, and W. Schattke, Phys. Rev. B **73**, 195406 (2006).